Bistable Reflection Assisted by Fano Resonance in DMDMW With Low-Threshold and Large Modulation Depth

ZhiXian Ni, Xianping Wang, Huiping Xu, Cheng Yin, Xin Xie, ChengYu Wu, Jun Li, Wen Yuan, and MingHuang Sang

***Abstract*—Owing to an additional thinner planar waveguide with micron scale is attracted to the symmetrical metal cladding waveguide (SMCW) with sub-millimeter scale, the interference interaction between different Q-value guided modes would generate a Fano reflectivity curve. In our double metal-dielectric-metal waveguides (DMDMW) structure, a Kerr nonlinear medium is located in the guiding layer of the SMCW where the excited oscillating wave is enormously enhanced. Numerical calculations show that a minute variation of the incident light intensity will give rise to a change in the dielectric constant of the Kerr nonlinear medium and lead to positive feedback. A bistable reflection can be achieved with a low threshold and a large modulation depth because of the sharpness and the asymmetricity of the Fano reflectivity curve.**

***Index Terms*—Optical bistability, physical optics.**

I. Introduction

OPTICAL bistability (OB) is characterized by an S-shaped hysteresis loop [1] and catches a widespread attention due to its intriguing applications in optical switching [2], optical storage [3] and optical diode [4]. Different from the external stimuli (such as the magneto-optical effect [5] and the electro-optic effect [6]), the all-optical bistability is an internal stimulus scheme, where a Kerr nonlinear medium or an absorber is utilized to induce a positive feedback and therefore the electronic bottleneck can be excellently avoided. There are two indicators to evaluate the performance of all-optical bistability, one is the threshold and the other is the modulation depth (MD). For reducing the threshold, various resonant configurations, including micro/nano photonic [7] and Fabry-Perot Cavity [8], have been adopted to enhance the light-matter interaction and then sharp the reflectivity curve. However, their productions need a high precision and thus a complex process.

The MD is defined as the difference between the logical "1" and "0" normalized by the incident power and it is difficult to obtain a large MD by using a symmetric resonance. Fano resonance, which is an asymmetric resonance interaction between continuous and discrete states or an interference pheromone between two different resonances, was firstly found in quantum [9] and subsequently explored in several optical systems (such as photonic crystals [10] and surface plasmon resonance [11]). The sharpness of the Fano reflectivity curve has been widely designed to magnify the sensing sensitivity [12] and enlarge the Goos-Hänchen shift [13]. Recently, the Fano resonance structure containing a Kerr nonlinear medium [14] was proposed to achieve the OB with both a low threshold and a large MD as a result of the sharpness and asymmetricity of the Fano reflectivity curve, respectively.

It is demonstrated that the ultrahigh-order modes [15] excited in a symmetrical metal-cladding waveguide (SMCW) are highly sensitive to the variation of structural parameters [16] and the generated oscillating wave in the guiding layer can enhance the light-matter interaction, e.g., the Raman scattering [17], the RGB lasing [18], and the optical bistability [19]. By adding a thinner planar waveguide on the SMCW, the so-called double metal-dielectric-metal waveguides (DMDMW) structure is formed and the realized asymmetric Fano reflectivity curve is capable of getting giant GH shifts with a strong reflected beam intensity [20]. Here, the DMDMW structure with a Kerr nonlinear medium inside the guiding layer of the SMCW is presented to achieve a bistable reflection with a low threshold and a large modulation depth (0.88). Evidently, the fabrication of our planar bistability scheme is quite simple. In addition, the relationship between different thicknesses of the kerr-nonlinear layer and threshold has been discussed.

II. Structure and Principles

As illustrated in Fig. 1, the schematic layout of the double metal-dielectric-metal waveguides (DMDMW) can be divided

Manuscript received 29 October 2022; revised 19 December 2022; accepted 30 December 2022. Date of publication 5 January 2023; date of current version 10 January 2023. This work was supported by the National Natural Science Foundation of China under Grants 12064017 and 11864017. *(Corresponding author: Xianping Wang.)*

ZhiXian Ni, Xianping Wang, Xin Xie, ChengYu Wu, Wen Yuan, and MingHuang Sang are with the Jiangxi Key Laboratory of Photoelectronics and Telecommunication, College of Physics and Communication Electronics, Jiangxi Normal University, Nanchang 330022, China (e-mail: 851071060@qq.com; xpwang@jxnu.edu.cn; 923123010@qq.com; 1402845850@qq.com; yuanwen@jxnu.edu.cn; 893119789@qq.com).

Huiping Xu is with the National Electrical and Electronic Experimental Teaching Demonstration Center, School of Electrical and Electronic Engineering, Huazhong University of Science and Technology, Wuhan 430074, China (e-mail: xuhuiping@hust.edu.cn).

Cheng Yin is with the Jiangsu Key Laboratory of Power Transmission and Distribution Equipment Technology, Hohai University, Changzhou 213022, China (e-mail: cyin.phys@gmail.com).

Jun Li is with the Department of Physics, Jiangxi Normal University Science and Technology College, Jiujiang 332020, China (e-mail: junlee@jxnu.edu.cn).

Digital Object Identifier 10.1109/JPHOT.2022.3233710

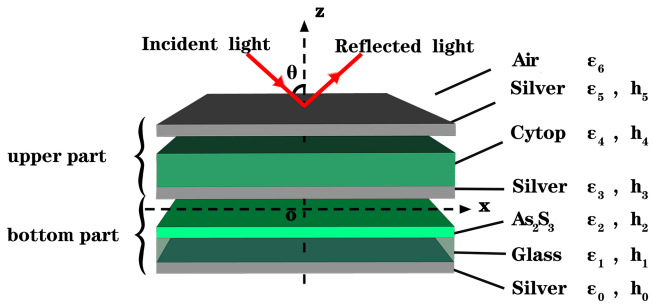

Fig. 1. Schematic of the DMDMW where the Kerr nonlinear medium (As_2S_3) is inside the guiding layer of the SMCW.

into two parts. The upper part is a three-layers waveguide structure, where Cytop is selected as the guiding layer and sandwiched by two thin metal films. The bottom part is a typical SMCW structure, whose guiding layer is composed of As_2S_3 and glass, both the coupling layers and the substrate are metal films. From top to down, their thicknesses are denoted as $h_5 = 50$ nm, $h_4 = 2.4$ μm, $h_3 = 60$ nm, $h_2 = 200$ nm, $h_1 = 0.5$ mm, and $h_0 = 300$ nm, respectively. All metal films are supposed to be silvers, whose dielectric constant ($\varepsilon_5 = \varepsilon_3 = \varepsilon_0 = -18 + 0.5i$ at $\lambda = 632.8$ nm) can be deduced from the Drude model. For the Kerr nonlinear medium (As_2S_3), its dielectric constant ε_2 is quadratically depended on the electric field intensity E_2 in the Kerr nonlinear medium [21]

$$\varepsilon_2 = \varepsilon_2^l + \chi^{(3)}|E_2|^2, \tag{1}$$

where $\varepsilon_2^l = 5.6644$ and $\chi^{(3)} = 3.12\times10^{-18}\text{m}^2/\text{V}^2$ are the linear part of dielectric constant and the Kerr nonlinear coefficient, respectively. The dielectric constant of air, Cytop and the glass are marked as $\varepsilon_6 = 1$, $\varepsilon_4 = 1.7956$ [22] and $\varepsilon_1 = 2.25$, respectively.

According to the Helmholtz equation, the distribution of the transverse electric field (TE) in each layer of DMDMW can be described as (2), shown at the bottom of this page [23]: where A_i and B_i are the electric amplitudes of the plane waves traveling upward and downward, $\alpha_i = k_0\sqrt{N^2 - \varepsilon_i}$ is the attenuation coefficient, $k_0 = 2\pi/\lambda$ is the wave vector, and λ is the light wavelength in vacuum, $N = \sqrt{\varepsilon_6}\sin\theta$ is the effective refractive index, θ is the angle of incidence, and $i = 0, 1, 2, 3, 4, 5, 6$ respectively.

Note that, the dielectric constants of Kerr nonlinear medium (As_2S_3)ε_2 are electric field intensity E_2 dependent, and the electric field intensity E_2 can be determined by a recursive computation. After all the dielectric constants of the DMDMW structure have been known, its reflection coefficient r can be calculated from the analytical transfer matrix method [24]

$$r = \frac{B_6}{A_6} = \frac{r_{65} + r_{543210}\exp(-2\alpha_5 h_5)}{1 + r_{65}\cdot r_{543210}\exp(-2\alpha_5 h_5)}, \tag{3}$$

where

$$r_{543210} = \frac{r_{10} + r_{54321}\exp(2i\alpha_1 h_1)}{1 + r_{10}\cdot r_{54321}\exp(2i\alpha_1 h_1)}, \tag{4}$$

$$r_{54321} = \frac{r_{21} + r_{5432}\exp(2i\alpha_2 h_2)}{1 + r_{21}\cdot r_{5432}\exp(2i\alpha_2 h_2)}, \tag{5}$$

Equation (6), shown at the bottom of this page, and $r_{ji} = (\alpha_j + \alpha_i)/(\alpha_j - \alpha_i)$ is the Fresnel reflection coefficient along each interface. The reflectivity is finally given by $R = |r|^2$.

The characteristic equation of the guided modes in two parts of the DMDMW can be expressed as (7), shown at the bottom of the next page [25]: where $\kappa_i = k_0\sqrt{\varepsilon_i - N^2}$ are the transverse wavenumbers in each layer, m and n are the mode order in the upper and the bottom part, respectively. By neglecting the nonlinear effect of As_2S_3, the relationship between TE-polarization reflectivity and the angle of incidence in the DMDMW is illustrated in Fig. 2(a). It is obvious that there exist three resonant dips ($\theta_1 = 18.003^\circ$, $\theta_2 = 18.212^\circ$ and $\theta_2 = 18.311^\circ$) in the marked red dash box. When the upper part is shined by a TE-polarization beam, the lowest TE mode is excited and contributes to a resonant dip at angle $\theta_2' = 18.017^\circ$ (see Fig. 2(b)). Because the thickness of guiding layer in the bottom part is extended into a sub-millimeter scale, the ultra-high order mode can be excited and there are two resonant dips ($\theta_1' = 17.990^\circ$ and $\theta_3' = 18.251^\circ$) locate in the marked red dash box (see Fig. 2(c)). When the upper part is attached to the bottom part, the lowest TE-polarization mode in upper part (the discrete state) will couple with the ultra-high order modes in the bottom part (the continuous state), and this combination leads to the

$$E_y(x) = \begin{cases} A_6\exp[-\alpha_6(x - h_3 - h_4 - h_5)] + B_6\exp[\alpha_6(x - h_3 - h_4 - h_5)], & h_3 + h_4 + h_5 < x < +\infty, \\ A_5\exp[-\alpha_5(x - h_3 - h_4)] + B_5\exp[\alpha_5(x - h_3 - h_4)], & h_3 + h_4 < x < h_3 + h_4 + h_5, \\ A_4\exp[-\alpha_4(x - h_3)] + B_4\exp[\alpha_4(x - h_3)], & h_3 < x < h_3 + h_4, \\ A_3\exp[-\alpha_3 x] + B_3\exp[\alpha_3 x], & 0 < x < h_3, \\ A_2\exp[-\alpha_2 x] + B_2\exp[\alpha_2 x], & -h_2 < x < 0, \\ A_1\exp[-\alpha_1(x + h_2)] + B_1[\alpha_1(x + h_2)], & -h_1 - h_2 < x < -h_2, \\ A_0\exp[-\alpha_0(x + h_1 + h_2)], & -\infty < x < -h_1 - h_2. \end{cases} \tag{2}$$

$$r_{5432} = \frac{r_{32} + r_{32}r_{43}r_{54}\exp(2i\alpha_4 h_4) + [r_{43} + r_{54}\exp(2i\alpha_4 h_4)]\exp\exp(2i\alpha_3 h_3)}{1 + r_{43}r_{54}\exp(2i\alpha_4 h_4) + r_{32}[r_{43} + r_{54}\exp(2i\alpha_4 h_4)]\exp\exp(2i\alpha_3 h_3)}, \tag{6}$$

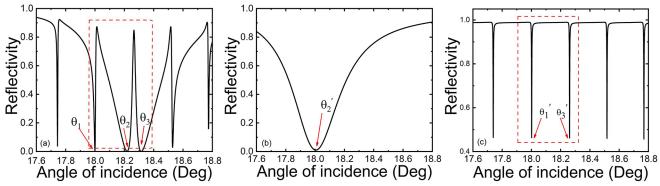

Fig. 2. The TE polarization reflectivity spectrum of (a) DMDMW, (b) Upper part, and (c) Bottom part.

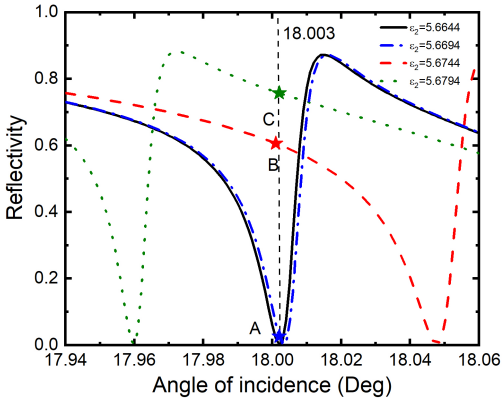

Fig. 3. Reflectivity of one selected dip as dielectric constant ε_2 increasing from 5.6644 to 5.6794 with a step of 0.005, and the black dash line indicates the angle of incidence is fixed at $\theta = 18.003^{\circ}$.

Fano resonances (shown in Fig. 2(a)). In detail, the head of the lowest TE-polarization at angle θ_2' overlaps the ultra-high mode at angle θ_1' and ultimately generate a sharp asymmetric Fano resonance reflectivity curve. Meanwhile, another asymmetric Fano resonance reflectivity curve is triggered by coupling the tail of the lowest TE-polarization at angle θ_2' with the ultra-high mode at angle θ_3'. It should be pointed out that the Q-value of the guided modes in both parts can be modulated by altering the thicknesses of their guiding layer and the coupling strength is closely linked to the thickness of the middle silver film.

III. Result and Discussion

To qualitatively estimate the high sensitivity of the Fano resonance excited in the DMDMW, one selected resonant dip is enlarged for more detailed analysis (shown in Fig. 3). As the dielectric constant ε_2 of the Kerr nonlinear medium (As_2S_3) increasing from 5.6644 to 5.6794 with a step of 0.005, the resonant dip of the ultra-high order mode excited in the SMCW will shift to the starboard side.

However, the resonant dip of the lowest TE-polarization mode in the upper part remains unaffected. Therefore, the coupling resulted Fano reflectivity curve will also move to the right. If the angle of incidence is fixed at $\theta_{in} = 18.003^{\circ}$, the reflectivity jumps from a small value (see point A in Fig. 3, blue star) to a high value (see point C in Fig. 3, green star). It means that the reflectivity of DMDMW structure can be easily modulated by the intensity of incident light because the Kerr nonlinear medium (As_2S_3) is placed inside the guiding layer of the SMCW.

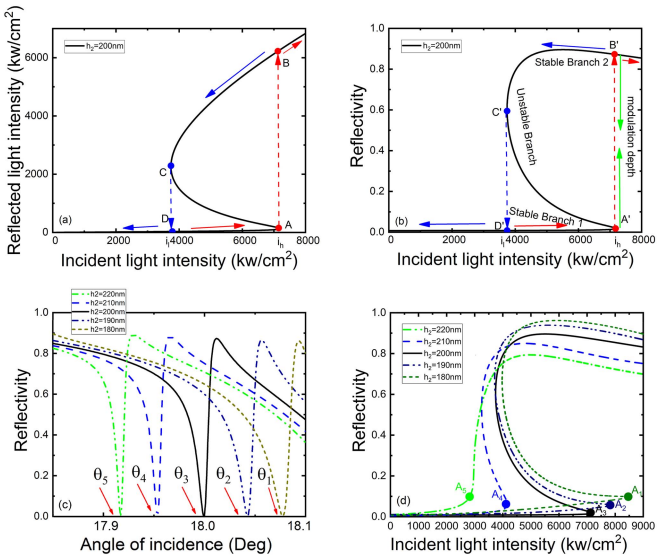

Fig. 4. (a)The reflected light intensity with respect to the incident light intensity at the incident angle at 18.003°, (b)The relationship between the reflectivity and incident light intensity, (c) Magnified fano resonance curve of different kerr-nonlinear layer thicknesses, (d)The relationship between the reflectivity and incident light intensity with different dimensions of kerr-nonlinear layer.

As shown in Fig. 4(a), when the angle of incidence is fixed at $\theta_{in} = 18.003^{\circ}$, there exists an S-shape relationship between the reflected light intensity and the incident light intensity. The low threshold intensity I_l (see point C) and the high threshold intensity I_h (see point A) are 3743 kw/cm^2 and 7150 kw/cm^2, respectively. To reveal the underline physics of OB, the reflectivity as a function of the incident light intensity is plotted in Fig. 4(b). Because the angle offset ($\Delta\theta = \theta_{in} - \theta_1 = 0.003^{\circ}$) between the fixed angle of incidence and the resonant angle θ_1 is set to be very small, the reflectivity initially near zero and the reflected light intensity increases approximately linear with the increasing incident light intensity along the stable branch 1. However, once the incident light intensity exceeds the high threshold intensity I_h, the reflected light intensity suddenly jumps to a big value (see point B). The reason is as follows: a majority of the incident light intensity is coupled into the DMDMW structure, the dielectric constant ε_2 of the Kerr nonlinear medium increases corresponding, and finally the Fano resonance reflectivity curve moves to the right side. The obtained MD is 0.88. We can similarly understand the principle of reflectivity variation along the stable branch 2 and the down-switch phenomenon at point C. Should be pointed out that the threshold is closely related to the angle offset and thickness of the Kerr nonlinear medium.

$$\begin{cases} \kappa_4 h_4 = m\pi + \arctan\left(\frac{\alpha_5}{\kappa_4}\right) + \arctan\left(\frac{\alpha_3}{\kappa_4}\right), & \text{for the upper part,} \\ \kappa_2 h_2 = n\pi + \arctan\left(\frac{\alpha_3}{\kappa_2}\right) + \arctan\left(\frac{\kappa_1}{\kappa_2}\tan\left[\arctan\left(\frac{\alpha_3}{\kappa_1}\right) - \kappa_1 h_1\right]\right), & \text{for the bottom part,} \end{cases} \tag{7}$$

In order to explore the relationship between thickness and threshold. The kerr-nonlinear layer thickness has been increased with the step of 10 nm, from $h_2 = 180$ nm to $h_2 = 220$ nm. As the kerr-nonlinear layer thickness increasing, the fano resonance curves of revised structure with different thickness are shown in Fig. 4(c). To detailed estimate the relationship between the kerr-nonlinear layer thickness and the threshold of bistable state, similar selected resonant dips is enlarged for more detail analysis (in Fig. 4(c)). θ_1 to θ_5 is the angle of incidence, which are selected from resonant dips in the five different fano resonce curves. In the simulation process, with the increasing thickness of the kerr-nonlinear layer, the low threshold intensity has a significant shift to the left (from A_1 to A_5). That's because thicker kerr-nonlinear layer induces stronger optical absorption [26]. Namely, thicker Kerr nonlinear medium leads to lower threshold intensity.

IV. Conclusion

In conclusion, by using the sharpness and asymmetricity properties of the Fano reflectivity resulted from the DMDMW structure, a bistable reflection simultaneously with a low threshold and a large modulation depth is achieved. The physical principle of the OB is discussed in detail. Our structure is quite simple and could have potential applications in all-optical switch and storage.

References

[1] H. Gibbs, *Optical Bistability: Controlling Light With Light*. Amsterdam, The Netherlands: Elsevier, 2012.

[2] K. Nozaki et al., "All-optical switching for 10-Gb/s packet data by using an ultralow-power optical bistability of photonic-crystal nanocavities," *Opt. Exp.*, vol. 23, no. 23, pp. 30379–30392, 2015.

[3] T. Tanabe, M. Notomi, S. Mitsugi, A. Shinya, and E. J. O. L. Kuramochi, "Fast bistable all-optical switch and memory on a silicon photonic crystal on-chip," *Opt. Lett.*, vol. 30, no. 19, pp. 2575–2577, 2005.

[4] X. Xia, X. Zhang, J. Xu, and Y. Yang, "Monoatomic optical diode based on direction-dependent bistability in the Purcell regime," *Optik*, vol. 167, pp. 95–102, 2018.

[5] S. Umegaki, H. Inoue, and T. Yoshino, "Optical bistability using a magneto-optic modulator," *Appl. Phys. Lett.*, vol. 38, no. 10, pp. 752–754, 1981.

[6] A. Witt, M. Wegener, C. Klingshirn, D. Gnass, and D. Jäger, "CdS photoelectric device: Modulation and optical bistability at 514 nm," *Appl. Phys. Lett.*, vol. 52, no. 5, pp. 342–344, 1988.

[7] Q. M. Ngo, K. Q. Le, and V. D. Lam, "Optical bistability based on guided-mode resonances in photonic crystal slabs," *J. Opt. Soc. Amer. B*, vol. 29, no. 6, pp. 1291–1295, 2012.

[8] K. Ikeda and Y. Fainman, "Nonlinear Fabry-Perot resonator with a silicon photonic crystal waveguide," *Opt. Lett.*, vol. 31, no. 23, pp. 3486–3488, 2006.

[9] U. Fano, "Effects of configuration interaction on intensities and phase shifts," *Phys. Rev.*, vol. 124, no. 6, 1961, Art. no. 1866.

[10] A. E. Miroshnichenko, S. Flach, and Y. S. Kivshar, "Fano resonances in nanoscale structures," *Rev. Modern Phys.*, vol. 82, no. 3, 2010, Art. no. 2257.

[11] N. Liu et al., "Plasmonic analogue of electromagnetically induced transparency at the Drude damping limit," *Nature Mater.*, vol. 8, no. 9, pp. 758–762, 2009.

[12] S. Hayashi, D. V. Nesterenko, and Z. Sekkat, "Fano resonance and plasmon-induced transparency in waveguide-coupled surface plasmon resonance sensors," *Appl. Phys. Exp.*, vol. 8, no. 2, 2015, Art. no. 022201.

[13] H. Saito, Y. Neo, T. Matsumoto, and M. Tomita, "Giant and highly reflective Goos-Hänchen shift in a metal-dielectric multilayer Fano structure," *Opt. Exp.*, vol. 27, no. 20, pp. 28629–28639, 2019.

[14] L. Y. Mario, S. Darmawan, and M. K. Chin, "Asymmetric Fano resonance and bistability for high extinction ratio, large modulation depth, and low power switching," *Opt. Exp.*, vol. 14, no. 26, pp. 12770–12781, 2006.

[15] H. Lu, Z. Cao, H. Li, and Q. Shen, "Study of ultrahigh-order modes in a symmetrical metal-cladding optical waveguide," *Appl. Phys. Lett.*, vol. 85, no. 20, pp. 4579–4581, 2004.

[16] T. Yu, H. Li, Z. Cao, Y. Wang, Q. Shen, and Y. He, "Oscillating wave displacement sensor using the enhanced Goos–Hänchen effect in a symmetrical metal-cladding optical waveguide," *Opt. Lett.*, vol. 33, no. 9, pp. 1001–1003, 2008.

[17] C. Yin et al., "Enhanced Raman scattering based on Fabry-Perot like resonance in a metal-cladding waveguide," *J. Raman Spectrosc.*, vol. 47, no. 5, pp. 560–564, 2016.

[18] H. Dai, C. Yin, Z. Xiao, Z. Cao, and X. Chen, "White beam lasing from a hybrid microcavity with slab-capillary mode coupling," *Phys. Rev. Appl.*, vol. 11, no. 6, 2019, Art. no. 064055.

[19] Y. Zhang et al., "Low-threshold bistable reflection assisted by oscillating wave interaction with Kerr nonlinear medium," *Chin. Phys. B*, vol. 30, no. 8, 2021, Art. no. 084203.

[20] K. Zhang et al., "Giant Goos-Hänchen shift with high reflectivity via double metal-dielectric-metal waveguides induced Fano resonance," *IEEE Photon. J.*, vol. 14, no. 1, pp. 1–5, 2021.

[21] V. G. Ta'eed et al., "Ultrafast all-optical chalcogenide glass photonic circuits," *Opt. Exp.*, vol. 15, no. 15, pp. 9205–9221, 2007.

[22] A. W. Wark, H. J. Lee, and R. M. Corn, "Long-range surface plasmon resonance imaging for bioaffinity sensors," *Anal. Chem.*, vol. 77, no. 13, pp. 3904–3907, 2005.

[23] K. Rollke and W. Sohler, "Metal-clad waveguide as cutoff polarizer for integrated optics," *IEEE J. Quantum Electron.*, vol. 13, no. 4, pp. 141–145, Apr. 1977.

[24] P. Su, Z. Cao, K. Chen, X. Deng, C. Liu, and Q. Shen, "Explicit expression of light reflection from inhomogeneous planar structures," *J. Opt. Soc. Amer. B*, vol. 24, no. 12, pp. 3077–3080, 2007.

[25] H. Zhou, X. Chen, P. Hou, and C.-F. Li, "Giant bistable lateral shift owing to surface-plasmon excitation in Kretschmann configuration with a Kerr nonlinear dielectric," *Opt. Lett.*, vol. 33, no. 11, pp. 1249–1251, 2008.

[26] W. Zhang and S. F. Yu, "Bistable switching using an optical Tamm cavity with a Kerr medium," *Opt. Commun.*, vol. 283, no. 12, pp. 2622–2626, 2010.